International Journal of Modern Physics E

Azimuthal anisotropy of strange and multi-strange hadrons in U+U collisions at $\sqrt{s_{NN}} = 193$ GeV at STAR

Vipul Bairathi
(For the STAR collaboration)
Instituto de Alta Investigación, Universidad de Tarapacá,
Arica 1000000, Chile
vipul.bairathi@gmail.com

We present systematic measurements of azimuthal anisotropy for strange hadrons (K_s^0, ϕ and Λ) and multi-strange hadrons (Ξ and Ω) at mid-rapidity ($|y| < 1.0$) in U+U collisions at $\sqrt{s_{NN}} = 193$ GeV using the STAR detector at the Relativistic Heavy Ion Collider (RHIC). Flow coefficients (v_2, v_3 and v_4) are presented as a function of transverse momentum (p_T) for minimum bias and three different centrality intervals. The η sub-event plane method is used to obtain the results. These measurements are compared with the published results from Au+Au collisions at $\sqrt{s_{NN}} = 200$ GeV. Number of Constituent Quark (NCQ) scaling of the measured flow coefficients in U+U collisions is discussed. We also present the ratio of v_n scaled by the participant eccentricity ($\varepsilon_n\{2\}$) to explore system size dependence and collectivity in U+U collisions. The measured flow coefficients are compared with hydrodynamic and transport model calculations.

Keywords: Azimuthal anisotropy; U+U collisions; NCQ scaling

PACS numbers: 25.75.Ld

1. Introduction

The fundamental theory of strong interactions is Quantum Chromodynamics (QCD).[1–3] Study of QCD in extreme temperature and density regimes can be done through the measurement of the properties of hot and dense medium produced in high-energy heavy-ion collisions. At these extreme conditions, the state of matter is in the form of quarks and gluons, which are no longer confined within the hadrons. This de-confined state of matter is known as Quark Gluon Plasma (QGP).[4,5] The goal of relativistic heavy-ion collision experiments is to create such a hot and dense state of matter and study its properties.

Azimuthal anisotropy of produced particles is one of the clearest experimental signature of the formation of QGP in relativistic heavy-ion collisions. Experimentally, the dynamics and collective behavior of the QGP medium produced in the collisions have been studied by the measurements of particle production in momentum space relative to the reaction plane.[6–9] The reaction plane is defined as the plane containing the beam direction and impact parameter vector between the two colliding nuclei. In non-central nucleus-nucleus collisions, the initial overlap region is spatially anisotropic with respect to the reaction plane. Multi-particle interactions among the constituents of the medium lead to a local thermalization, which creates a pressure gradient throughout the system. Due to this pressure gradient, the initial geometrical anisotropy converts into the momentum space anisotropy, which is reffered as anisotropic flow. The anisotropy diminishes with the expansion and cooling down of the system with time. Due to the self-quenching nature, the azimuthal anisotropy provides useful information of the early stages of heavy-ion collisions.[10,11]

Azimuthal anisotropy is generally described by a Fourier expansion of the azimuthal angle distribution of the produced particles with respect to the reaction plane in the following form:[12,13]

$$\frac{dN}{d\phi} \propto 1 + \sum_{n=1}^{\infty} 2v_n \cos[n(\phi - \psi_{RP})]. \tag{1}$$

The Fourier coefficients v_n are known as flow coefficients, ϕ is the azimuthal angle and ψ_{RP} is the reaction plane angle. In experiments, the flow coefficients are measured with respect to the event plane angle ψ_n as $v_n = \langle \cos[n(\phi - \psi_n)] \rangle$.

The second harmonic coefficient v_2 indicates the strength of the elliptic flow generated due to the anisotropic geometry of initial overlap region. Therefore, the measured v_2 reflects the equation of state of the QGP medium produced in the collisions.[14] Strange hadrons, especially multistrange hadrons, because of their small hadronic interaction cross sections and freeze-out temperatures close to the phase transition temperature, are believed to be less sensitive to hadronic re-scatterings in the late stage of collisions and thus serve as a good probe for the partonic stage in heavy-ion collisions.[15,16]

The higher order flow harmonics ($v_n > 2$) are expected to be created by fluctuations in the participant positions and the initial collision geometry.[17] Strength of these fluctuations strongly depends on the initial conditions of heavy-ion collisions, therefore measurement of higher order flow harmonics can help to constrain the initial conditions of theoretical models. The results on elliptic flow of various identified hadrons from Au+Au collisions at RHIC have successfully demonstrated the collective behavior of the medium produced in heavy-ion collisions.[18–20] Measurements of higher order flow harmonics have also provided valuable insight for a precise extraction of transport properties of the QGP.[21,22]

In this work, we present the results on flow coefficients v_n (n = 2, 3 and 4) of K_s^0, ϕ, Λ, Ξ and Ω at mid-rapidity in collisions of deformed shape Uranium nuclei. Uranium nuclei have a prolate shape.[23] Therefore, depending on the angles of the two colliding Uranium nuclei relative to the reaction plane, several collision configurations of U+U collisions are possible.[24–27] Study of different collision configurations will help in constraining the initial conditions in models.[28–30] It has also been shown that the energy density could be increased even further in U+U collisions compared to Au+Au collisions to test ideal hydrodynamic behavior of the elliptic flow.[24]

2. Detector Setup and Analysis

In this work, we present results for minimum bias U+U collisions at $\sqrt{s_{NN}}$ = 193 GeV data set collected by the STAR experiment during the year 2012. The minimum bias triggered events with a primary collision vertex position along the longitudinal beam direction (V_z) within 30 cm from the center of the detector are selected for this analysis. An additional selection on the transverse position of the primary vertex radius ($V_r < 2.0$ cm) from the center of the beam pipe is also used to minimize effects of beam pipe interactions. The centrality selection of events is based on the measured charged particle multiplicity from the TPC within pseudorapidity $|\eta| < 0.5$. This multiplicity is known as reference multiplicity. The measured reference multiplicity distribution is compared with a Monte-Carlo Glauber Model[31] to get centrality of an event. Minimum bias collisions correspond to the centrality interval 0-80% while most central, mid-central, and peripheral collisions correspond to the 0-10%, 10-40%, and 40-80% centrality interval, respectively. After the event selection criteria, a total of ∼270 million good minimum-bias events are used for the analysis.

The main tracking detector, Time Projection Chamber (TPC)[32] of the STAR experiment is used for the particle identification. The TPC is capable of tracking charged particles within full azimuthal (2π) coverage and in uniform pseudorapidity ($|\eta| < 1.0$). The specific ionisation energy loss ($\langle dE/dx \rangle$) information is used to identify particles by comparing them with the theoretical predictions using Bichsel functions.[33] The TPC also provides momentum measurement of the charged particle tracks. It can identify pion and kaon tracks up to $p_T \approx 0.8$ GeV/c, and protons up to $p_T \approx 1.0$ GeV/c. In addition to the TPC, a Time Of Flight (TOF)[34–36] detector is used to extend the identification at higher p_T. It covers a pseudorapidity range of $|\eta| < 0.9$ with full azimuthal acceptance.

Strange and multi-strange hadrons (K_s^0, ϕ, Λ, Ξ and Ω) are reconstructed using the charged particle tracks from the TPC within pseduorapidity $|\eta| < 1.0$. Basic selection criteria for the charged particle tracks ($\pi^{\pm}$, $K^{\pm}$, and $p(\bar{p})$), as used in the previous published STAR papers,[18,20,37,38] are applied to ensure good quality of the tracks. Invariant mass technique is used to reconstructed strange and multi-strange hadrons along with various topological and kinematical selection criteria to reduce combinatorial background.[37,39]

3. Flow Analysis Technique

The η sub-event plane method is used to measure flow coefficients (v_n). In order to minimize the effects of non-flow correlations with the event plane, only charged particle tracks with a transverse momentum range of $0.2 < p_T < 2.0$ GeV/c are selected for the reconstruction of the angle ψ_n. The angle ψ_n calculated from the particles in an event is an estimate of the reaction plane angle, and is known as event plane angle. The event plane angle resolution with respect to the reaction plane is defined as,[12,13]

$$R = \langle \cos[n(\psi_n - \psi_{RP})] \rangle. \tag{2}$$

Since the reaction plane angle ψ_{RP} is unknown, the event plane resolution R cannot be directly calculated from this equation. Therefore, the resolution is estimated by correlating event planes calculated from two subsets of tracks, called sub-events A and B. The two sub-events are based on the pseudorapidity of a track. An η gap of $\Delta\eta = 0.1$ is introduced between the positive and negative pseudorapidity sub-events to suppress non-flow effects. The event plane resolution with the assumption of only flow correlations between the sub-events is calculated by the equation,[12,13]

$$\langle \cos[n(\psi_n - \psi_{RP})] \rangle = \sqrt{\langle \cos[n(\psi_n^A - \psi_n^B)] \rangle} \tag{3}$$

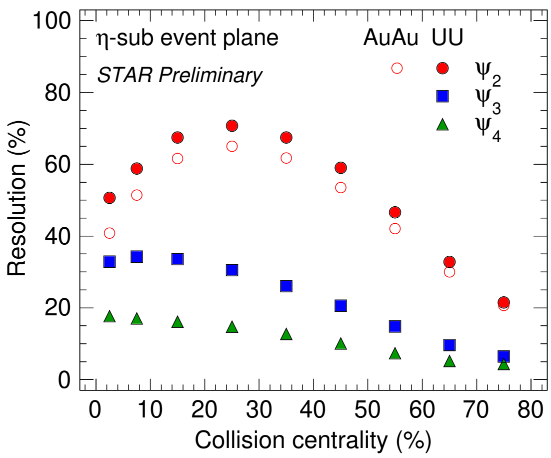

Fig. 1. η sub-event plane resolution as a function of centrality for ψ_2, ψ_3 and ψ_4 in U+U collisions at $\sqrt{s_{NN}} = 193$ GeV. For comparison, ψ_2 resolution from Au+Au collisions at $\sqrt{s_{NN}} = 200$ GeV is also shown.[40]

Figure 1 shows the η sub-event plane resolution as a function of centrality for ψ_2, ψ_3 and ψ_4 in U+U collisions at $\sqrt{s_{NN}} = 193$ GeV. The ψ_2 resolution is compared with Au+Au collisions at $\sqrt{s_{NN}} = 200$ GeV.[40] The shape of event plane resolution as a function of centrality in U+U collisions is similar to that of Au+Au collisions. Resolution is higher in U+U collisions compared to Au+Au collisions likely due to higher particle multiplicity in U+U collisions. For combined centrality classes i.e. 0-10%, 10-40% and 40-80%, an average resolution weighted by the raw-yield of particles of interest is calculated to correct flow coefficients. The measured flow coefficients v_n^{obs} are corrected by dividing the corresponding event plane resolution to get the final v_n coefficients as,

$$v_n = \frac{v_n^{obs}}{\sqrt{\langle \cos[n(\psi_n^A - \psi_n^B)] \rangle}}. \quad (4)$$

4. Results

In this section, we present results on flow coefficients of strange and multi-strange hadrons as a function of transverse momentum (p_T) at mid-rapidity ($|y| < 1$) for minimum bias and various centrality classes in U+U collisions at $\sqrt{s_{NN}} = 193$ GeV.

4.1. *p_T-dependence of flow coefficients*

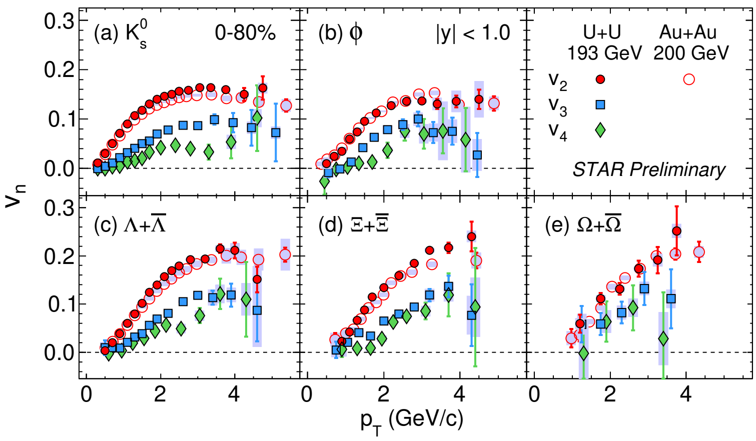

Fig. 2. Flow coefficients v_2, v_3 and v_4 of (a) K_s^0, (b) ϕ, (c) Λ, (d) Ξ, and (e) Ω at mid-rapidity ($|y| < 1$) for 0-80% centrality in U+U collisions at $\sqrt{s_{NN}} = 193$ GeV. The error bars represent statistical uncertainties. The bands represent point by point systematic uncertainties. For comparison, published results for v_2 from Au+Au collisions at $\sqrt{s_{NN}} = = 200$ GeV are shown by open circles.[19, 20]

Figure 2 represents p_T-dependence of flow coefficients $v_n(p_T)$ ($n = 2, 3, 4$) for K_s^0, ϕ, Λ, Ξ, and Ω at mid-rapidity ($|y| < 1$) in minimum bias U+U collisions at $\sqrt{s_{NN}} = 193$ GeV. The flow coefficients show an increasing trend with p_T reaching a maximum value and then saturate for the intermediate p_T region. The maximum value of v_n for different particles seems to have a mass dependence. It takes place at relatively higher p_T for heavier particles compare to lighter particles. The magnitude of v_2 is greater than v_3 and v_4 in minimum bias U+U collisions. The non-zero values of higher-order flow coefficients for the measured p_T range is an indication of event-by-event fluctuations in the initial energy density profile. The dependence of elliptic flow v_2 on p_T in minimum bias U+U collisions is similar to that observed in Au+Au collisions at $\sqrt{s_{NN}} = 200$ GeV.

4.2. *Centrality dependence of flow coefficients*

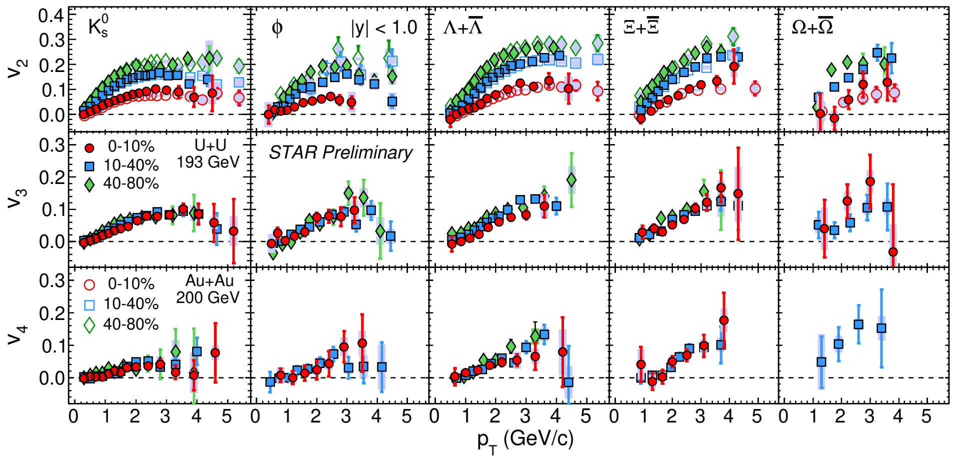

Fig. 3. v_n coefficients as a function of p_T for K_s^0, ϕ, Λ, Ξ, and Ω at mid-rapidity ($|y| < 1$) in U+U collisions at $\sqrt{s_{NN}} = 193$ GeV for centrality classes 0-10%, 10-40% and 40-80%. The error bars represent statistical uncertainties. The bands represent point by point systematic uncertainties. For comparison, published results for v_2 from Au+Au collisions at $\sqrt{s_{NN}} = 200$ GeV are shown by open markers.[19,20]

Figure 3 shows dependence of flow coefficients $v_n(p_T)$ on collision centrality for K_s^0, ϕ, Λ, Ξ, and Ω in U+U collisions at $\sqrt{s_{NN}} = 193$ GeV. The results are presented for three centrality intervals 0-10% (most-central), 10-40% (mid-central), and 40-80% (peripheral). A clear centrality dependence of elliptic flow v_2 is observed in U+U collisions similar to that in Au+Au collisions measured by the STAR experiment.[19,20] The v_2 magnitude is found larger in peripheral collisions compared to the most central collisions for all particles. The dependence is expected as the eccentricity of the initial overlap region of the colliding nuclei increases from central to peripheral collisions. A weak centrality dependence of v_3 is observed, which is even weaker for v_4 in comparison to v_2. The lack of clear centrality dependence of higher order flow coefficients reflects the fact that the event-by-event fluctuations are the dominant source for the origin of triangular and quadrangular shape of the initial collision region.

4.3. *Eccentricity scaling*

In this section, we present flow coefficients scaled by the initial spatial eccentricity to explore the dependence of final state momentum space anisotropy on the initial collision geometry in heavy-ion collisions. The n^{th}-order participant eccentricity

(ε_n) is calculated by,[41,42]

$$\varepsilon_n = \frac{\sqrt{\langle r^n \cos(n\phi_{part})\rangle^2 + \langle r^n \sin(n\phi_{part})\rangle^2}}{\langle r^n \rangle}, \tag{5}$$

where r and ϕ_{part} are the positions of participating nucleons in the polar coordinate system shifted to the center of mass of the participating nucleons and n is the order of eccentricity. The angular bracket $\langle\rangle$ denotes an average over the participant nucleons in each event. The root mean square participant eccentricity is defined as $\varepsilon_n\{2\} = \sqrt{\langle\langle \varepsilon_n^2 \rangle\rangle}$, where the double angular bracket $\langle\langle\rangle\rangle$ denotes an average over the event ensemble. The values of $\varepsilon_n\{2\}$ are calculated using the Monte Carlo Glauber model[43,44] for different centrality intervals in U+U collisions at $\sqrt{s_{NN}}$ = 193 GeV. Deformation of Uranium nuclei has been taken into account in the Glauber model.

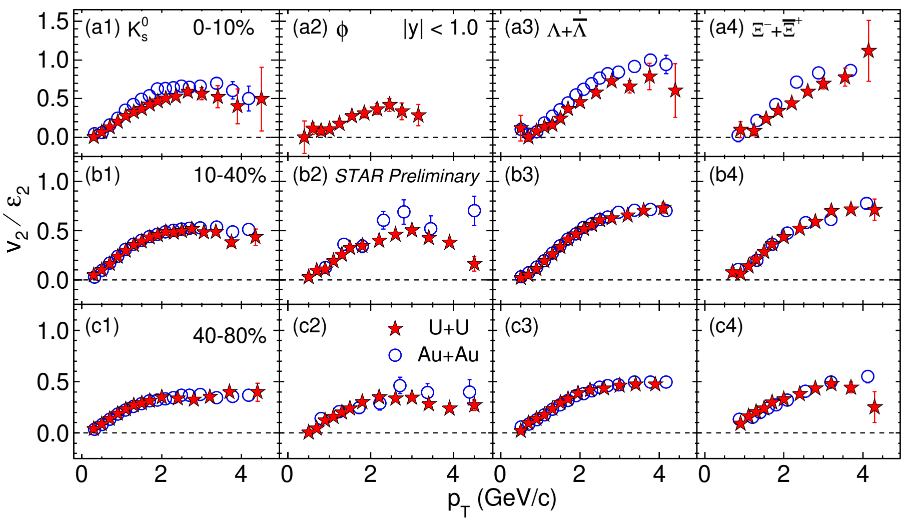

Fig. 4. v_2 scaled by participant eccentricity ε_2 as a function of p_T for K_s^0, ϕ, Λ, Ξ, and Ω in U+U collisions at $\sqrt{s_{NN}}$ = 193 GeV for centrality intervals 0-10%, 10-40% and 40-80%. The error bars represent statistical uncertainties. For comparison, published results for v_2/ε_2 from Au+Au collisions at $\sqrt{s_{NN}}$ = 200 GeV are shown by open markers.[19,20]

Figure 4 shows the ratio v_2/ε_2 for various particle species in U+U collisions at $\sqrt{s_{NN}}$ = 193 GeV. The published measurements in Au+Au collisions from the STAR experiment have reported a larger value of the ratio v_2/ε_2 in central collisions compared to the peripheral collisions, which suggests development of stronger collectivity in more central collisions.[45] We observed a similar magnitude of the ratio v_2/ε_2 in mid-central (10-40%) and peripheral collisions (40–80%) in both U+U and Au+Au collisions. However, comparison in most central collisions (0-10%) shows reverse trend than our expectation that v_2/ε_2, which is a measure of collectivity, should be higher in U+U collisions compared to Au+Au collisions. A similar observation is reported in the recently published article.[46] This suggests that additional dynamics, such as initial collision configurations, may also need to be taken into account in determining the collectivity in collisions of highly deformed nuclei such as Uranium.

4.4. *Number of constituent quark scaling*

The number of constituent quark (NCQ) scaling was first observed for identified particle v_2 at intermediate p_T in Au+Au collisions at RHIC.[20,38,47,48] It is shown that v_2 values scaled by the number of constituent quarks (n_q) as a function of transverse kinetic energy per constituent quark (KE_T/n_q) fall on a single curve for all particle species. This NCQ scaling is thought to be an indication for the development of collective flow during the QGP phase of the medium created in heavy-ion collisions.

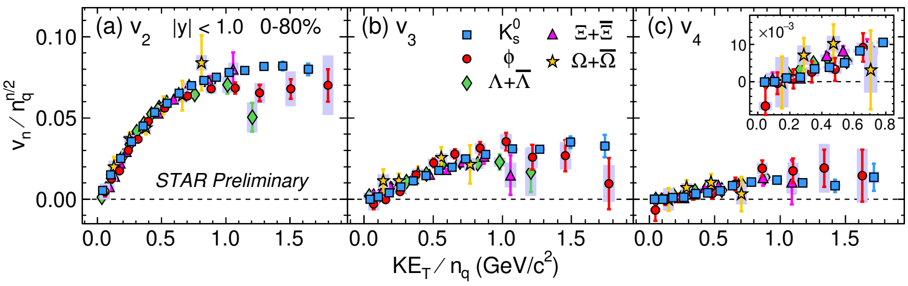

Fig. 5. Flow coefficients v_n scaled by number of constituent quarks (n_q) to the power $n/2$ as a function of transverse kinetic energy per constituent quark KE_T/n_q in minimum bias U+U collisions at $\sqrt{s_{NN}}$ = 193 GeV. The error bars represent statistical uncertainties. The bands represent point by point systematic uncertainties.

Figure 5 shows v_n coefficients scaled by $n_q^{n/2}$ as a function of KE_T/n_q, for various particles in U+U collisions $\sqrt{s_{NN}} = 193$ GeV. The transverse kinetic energy is defined as $KE_T = m_T - m_0$, where $m_T = \sqrt{p_T^2 + m_0^2}$ and m_0 is rest mass of the hadron. The NCQ scaling for current measurements holds within ±15% for all the particle species and for all flow harmonics in U+U collisions. This NCQ scaling suggests hadron production through quark coalescence or parton recombination in the intermediate p_T range (2.0 GeV/c $< p_T <$ 4.0 GeV/c).[49,50] Although, there are large differences in the collision geometry between U+U and Au+Au collisions, but the quark coalescence mechanism for hadron formation remains key features for the QGP medium created in heavy-ion collisions.

4.5. *Model comparisons*

In this section, we compare v_n coefficients measured in U+U collisions to the hydrodynamic and transport model calculations. The hydrodynamical model is based on the event-by-event 3+1 dimensional hydrodynamical calculations with a lattice QCD equation of state and $\eta/s = 0$.[51] The hydrodynamical calculations describe the mass ordering of v_n coefficients at low-p_T ($p_T < 2$ GeV/c).[52,53] It predicts the p_T and centrality dependence of flow coefficients in the relatively low-p_T region. Although, it deviates significantly from the data at higher p_T region, which shows a need of viscous corrections to the ideal hydrodynamical model.

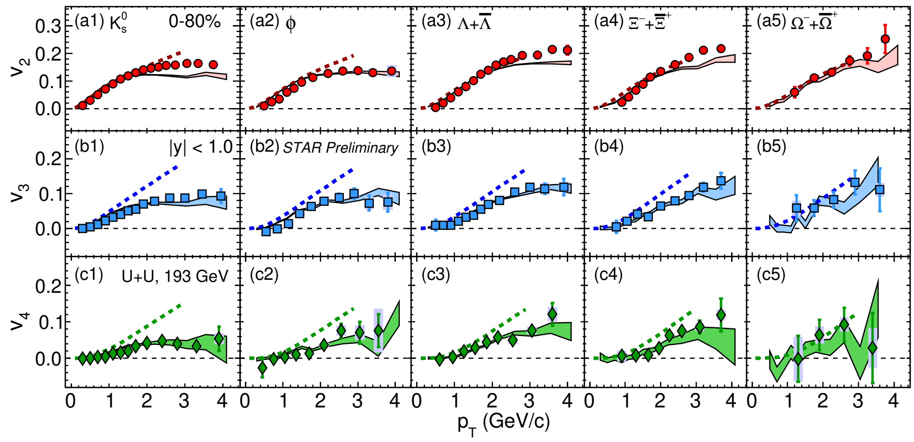

Fig. 6. Flow coefficients $v_n(p_T)$ for strange and multi-strange hadrons at mid-rapidity ($|y| < 1$) in minimum bias (0-80%) U+U collisions at $\sqrt{s_{NN}} = 193$ GeV compared with AMPT string melting and ideal hydrodynamic model calculations. AMPT model results are shown by colored bands while ideal hydrodynamic results are shown by colored dashed lines.

We also compared the v_n measurements to the string melting (SM) version of the AMPT model.[54–56] The AMPT-SM model incorporates both partonic and hadronic interactions. The U+U collision events are generated using a parton-parton scattering cross-section of 3 mb in the AMPT model. The model is modified to incorporate the deformation (prolate shape) of Uranium nucleus. Various initial state collision configurations of deformed Uranium nucleus e.g. tip-tip, body-body, and body-tip are implemented in the model. Details of the implementation and deformation parameter can be found in Refs. 26, 27. For the current analysis, a total of ~5 million minimum bias U+U collisions without selection of specific configurations are used.

The AMPT-SM model agrees well with the v_n measurements from U+U collisions data for all particle species within statistical uncertainties. It predicts mass ordering at low-p_T and a hadron type dependence in the intermediate p_T region similar to the experimental measurements. It also reproduces the p_T and centrality dependence of v_n coefficients in U+U collisions at $\sqrt{s_{NN}} = 193$ GeV.

5. Summary and Conclusions

We present measurements of $v_n(p_T)$ (n = 2,3,4) coefficients for K_s^0, ϕ, Λ, Ξ, and Ω at mid-rapidity for minimum bias and various centrality intervals in U+U collisions at $\sqrt{s_{NN}}$ = 193 GeV from the STAR experiment at RHIC. This work is recently published in Physical Review C.[57] We compared with our published elliptic flow v_2 results from Au+Au collisions at $\sqrt{s_{NN}}$ = 200 GeV. The v_2 values increase from central to peripheral collisions for all particle species in U+U collisions similar to those observed in Au+Au collisions at RHIC. Higher order flow harmonics show a less pronounced increase compared to v_2, which reflects dominance of collision geometry on the origin of elliptic flow. This may also indicate origin of higher order flow harmonics through event-by-event fluctuations in the initial energy density distribution of participating nucleons. We also compared v_n measurements with the ideal hydrodynamical and transport model calculations. The model calculations predict the same mass ordering at low p_T as in the experimental data. The ideal hydrodynamical calculations over-predict the values of flow coefficients at higher $p_T > 2$ GeV/c, which suggests the need for viscous correction to the model. The AMPT-SM model calculations agree well with the measurements within statistical uncertainties. We also observed NCQ scaling of v_2 in the intermediate p_T region for strange and multi-strange hadrons, which are expected to have small hadronic interaction cross-sections. The higher-order flow harmonics show a modified NCQ scaling, i.e. v_n scaled by $n_q^{n/2}$ follows a common trend for all particles as a function of KE_T/n_q. The sizable v_2 values for multi-strange hadrons exhibit collectivity of the medium produced in U+U collisions at RHIC.

Acknowledgments

We acknowledge Dr. Victor Roy for providing the hydrodynamical model results.

References

1. David J. Gross and Frank Wilczek, *Phys. Rev. Lett.* **30**, 1343 (1973).
2. David J. Gross and Frank Wilczek, *Phys. Rev. D* **8**, 3633 (1973).
3. H. D. Politzer, *Phys. Rev. Lett.* **30**, 1346 (1973).
4. E. V. Shuryak, *Phys. Rep.* **61**, 71-158 (1980).
5. L. D. McLerran, *Rev. Mod. Phys.* **58**, 1021 (1986).
6. BRAHMS Collaboration (I. Arsene *et al.*), *Nucl. Phys. A* **757**, 1 (2005).
7. PHOBOS Collaboration (B. B. Back *et al.*), *Nucl. Phys. A* **757**, 28 (2005).
8. STAR Collaboration (J. Adams *et al.*), *Nucl. Phys. A* **757**, 102 (2005).
9. PHENIX Collaboration (K. Adcox *et al.*), *Nucl. Phys. A* **757**, 184 (2005).
10. H. Sorge, *Phys. Rev. Lett.* **78**, 2309 (1997).
11. H. Sorge, *Phys. Rev. Lett.* **82**, 2048 (1999).
12. S. Voloshin and Y. Zhang, *Z. Phys. C* **70**, 665 (1996).
13. A. Poskanzer and S. Voloshin, *Phys. Rev. C* **58**, 1671 (1998).
14. R. Snellings, *New Journal of Physics* **13**, 055008 (2011).
15. A. Shor, *Phys. Rev. Lett.* **54**, 1122 (1985).
16. H. Hecke *et al.*, *Phys. Rev. Lett.* **81**, 5764 (1998).

17. B. Alver and G. Roland, *Phys. Rev. C* **81**, 054905 (2010).
18. STAR Collaboration (J. Adams *et al.*), *Phys. Rev. C* **72**, 014904 (2005).
19. STAR Collaboration (B. I. Abelev *et al.*), *Phys. Rev. C* **77**, 054901 (2008).
20. STAR Collaboration (L. Adamczyk *et al.*), *Phys. Rev. Lett.* **116**, 062301 (2016).
21. PHENIX Collaboration (A. Adare *et al.*), *Phys. Rev. Lett.* **107**, 252301 (2011).
22. STAR Collaboration (L. Adamczyk *et al.*), *Phys. Rev. C* **88**, 014904 (2013).
23. S. Raman, C. W. Nestor, and P. Tikkanen, *Atom. Data Nucl. Data Tabl.* **78**, 1 (2001).
24. C. Nepali, G. Fai and D. Keane, *Phys. Rev. C* **73**, 034911 (2006).
25. C. Nepali, G. Fai and D. Keane, *Phys. Rev. C* **76**, 051902(R) (2007).
26. Md. Rihan Haque, Z.-W. Lin, and B. Mohanty, *Phys. Rev. C* **85**, 034905 (2012).
27. V. Bairathi, Md. Rihan Haque, and B. Mohanty, *Phys. Rev. C* **91**, 054903 (2015).
28. U. Heinz and A. Kuhlman, *Phys. Rev. Lett.* **94**, 132301 (2005).
29. A. Kuhlman and U. Heinz, *Phys. Rev. C* **72**, 037901 (2005).
30. A. Kuhlman, U. W. Heinz and Y. V. Kovchegov, *Phys. Lett. B* **638**, 171 (2006).
31. M. Miller, K. Reygers, S. Sanders and P. Steinberg, *Ann. Rev. Nucl. Part. Sci.* **57**, 205 (2007).
32. M. Anderson *et al.*, *Nucl. Instrum. Meth. A* **499**, 659 (2003).
33. H. Bichsel, *Nucl. Instrum. Meth. A* **562**, 154 (2006).
34. W. J. Llope *et al.*, *Nucl. Instrum. Meth. A* **522**, 252 (2004).
35. W. J. Llope *et al.*, *Nucl. Instrum. Meth. A* **759**, 23 (2014).
36. J. Wu *et al.*, *Nucl. Instrum. Meth. A* **538**, 243 (2005).
37. STAR Collaboration (J. Adams *et al.*), *Phys. Rev. Lett.* **92**, 052302 (2004).
38. STAR Collaboration (J. Adams *et al.*), *Phys. Rev. Lett.* **95**, 122301 (2005).
39. STAR Collaboration (C. Adler *et al.*), *Phys. Rev. Lett.* **89**, 132301 (2002).
40. STAR Collaboration (L. Adamczyk *et al.*), *Phys. Rev. C* **94**, 034908 (2016).
41. B. Alver and G. Roland, *Phys. Rev. C* **81**, 054905 (2010).
42. D. Teaney and L. Yan, *Phys. Rev. C* **83**, 064904 (2011).
43. B. Alver, M. Baker, C. Loizides, P. Steinberg, *arXiv*:0805.4411 [nucl-ex].
44. C. Loizides, J. Nagle, P. Steinberg, *SoftwareX* **1-2**, 13 (2015).
45. STAR Collaboration (B. I. Abelev *et al.*), *Phys. Rev. C* **81**, 044902 (2010).
46. Md. Rihan Haque, Md. Nasim, and B. Mohanty, *J. Phys. G: Nucl. Part. Phys.* **46**, 085104 (2019).
47. PHENIX Collaboration (S. S. Adler *et al.*), *Phys. Rev. Lett.* **91**, 182301 (2003).
48. PHENIX Collaboration (A. Adare *et al.*), *Phys. Rev. Lett.* **98**, 162301 (2007).
49. D. Molnar and S. Voloshin, *Phys. Rev. Lett.* **91**, 092301 (2003).
50. R. Fries, B. Müller, C. Nonaka, and S. Bass, *Phys. Rev. Lett.* **90**, 202303 (2003).
51. V. Roy, *Private Communication* (2018).
52. C. Nonaka, R. Fries, and S. Bass, *Phys. Lett. B* **583**, 73 (2004).
53. T. Hirano and Y. Nara, *Phys. Rev. C* **69**, 034908 (2004).
54. B. Zhang, C. M. Ko, B.-A. Li, and Z.-W. Lin, *Phys. Rev. C* **61**, 067901 (2000).
55. Z.-W. Lin *et al.*, *Phys. Rev. C 64*, 011902 (2001).
56. Z.-W. Lin *et al.*, *Phys. Rev. C 72*, 064901 (2005).
57. STAR Collaboration (M. S. Abdallah *et al.*), *Phys. Rev. C* **103**, 064907 (2021).